BNL-93861-2010

What Do s- and p-Wave Neutron Average Radiative Widths Reveal?

S.F.Mughabghab;

National Nuclear Data Center, Brookhaven National Laboratory, Upton, NY 11793, USA
E-mail : mugabgab@bnl.gov

Presented at the
International Conference on Nuclear Data for Science and Technology

April 2010

National Nuclear Data Center
Brookhaven National Laboratory
P.O. Box 5000
Upton, NY 11973-5000
www.nndc.bnl.gov

DISCLAIMER

International Conference on Nuclear Data for Science and Technology 2010

WHAT DO S- AND P-WAVE NEUTRON AVERAGE RADIATIVE WIDTHS REVEAL?

S.F. Mughabghab
National Nuclear Data Center, Brookhaven National Laboratory, Upton, NY 11973-5000, U.S.A.
E-mail : mugabgab@bnl.gov

Received
Accepted for Publication

A first observation of two resonance-like structures at mass numbers 92 and 112 in the average capture widths of the p-wave neutron resonances relative to the s-wave component is interpreted in terms of a spin-orbit splitting of the 3p single-particle state into $p_{3/2}$ and $p_{1/2}$ components at the neutron separation energy. A third structure at about A=124, which is not correlated with the 3p-wave neutron strength function, is possibly due to the Pygmy Dipole Resonance. Five significant results emerge from this investigation: (i) The strength of the spin-orbit potential of the optical-model is determined as 5.7 ± 0.5 MeV, (ii) Non-statistical effects dominate the p-wave neutron-capture in the mass region A = 85 - 130, (iii) The background magnitude of the p-wave average capture-width relative to that of the s-wave is determined as 0.50 ± 0.05, which is accounted for quantitatively in terms of the generalized Fermi liquid model of Mughabghab and Dunford,(iv) The p-wave resonances are partially decoupled from the giant-dipole resonance (GDR), and (v) Gamma-ray transitions, enhanced over the predictions of the GDR, are observed in the ^{90}Zr - ^{98}Mo and Sn-Ba regions.

KEYWORDS : S- and P-wave Neutron Resonance Capture Widths, Spin-Orbit Potential, Valence Neutron Capture, Enhanced Gamma-ray Transitions, Gamma-ray Strength Functions, Giant Dipole Resonance, Pygmy Dipole Resonance

1. INTRODUCTION

More than half a century ago, Feshbach, Porter, and Weisskopf [1] explained the gross structure found in neutron cross sections as a function of neutron energy, as well as the s-wave neutron strength functions as a function of mass number, in terms of a model wherein the nucleus is replaced by a one-body complex-potential $V = V_0 + iW$ that interacts with the incident neutron. One prediction of this model relevant to this investigation is that the p-wave neutron strength-function maxima are obtained at mass numbers A = 27, 90, and 216 for a real potential-well depth V_0 = 42.0 MeV and $R = 1.45A^{1/3}$ fm [1]. By including a spin-orbit term in more realistic potentials that are coupled to the vibrational and rotational motion of the nucleus, the predicted 3p strength function did not split into $3p_{1/2}$ and $3p_{3/2}$ components [2]. Subsequent analysis of extensive p-wave strength function data [3,5], in terms of the Buck-Perey formulation [2] revealed a central peak at about A = 95, followed by a shoulder extending from A = 100 – 110. In contrast, neutron differential elastic scattering measurements and analysis in terms of R-matrix theory [6,7] successfully derived the $3p_{1/2}$ and $3p_{3/2}$ components of the 3p neutron strength functions, $S^1_{1/2}$ and $S^1_{3/2}$, for spin-zero target nuclei, and showed that their maxima are separated by ΔA = 17 ± 4. However, experimental difficulties generated large uncertainties in the $S^1_{1/2}$ values, compromising the location of the maximum for this component.

This investigation presents new evidence for the spin-orbit splitting of the 3p single-particle state at the neutron threshold. This finding is based on a novel method, developed here, which depends on the average capture widths of p-wave resonances derived from available neutron capture measurements in the unresolved resonance energy region, 3-500 keV. In addition, the generalized Fermi liquid model [8], modified to compute the average p-wave radiative widths in the mass regions above A = 140, is introduced to give additional support for the interpretation of the present results. The partial decoupling of p-wave resonances from the giant dipole resonance, which facilitates observations of non-statistical effects in the vicinity of the 3p neutron strength function, is briefly discussed.

2. METHODS

Presently, high-precision capture cross section data are available from various neutron facilities: The van-de-Graaf accelerator at Forschungzentrum at Karlsruhe, the electron linear accelerator at Oak Ridge National Laboratory, the van-de-Graaf accelerator at the Tokyo Institute of Technology, and the spallation neutron source at CERN; examples

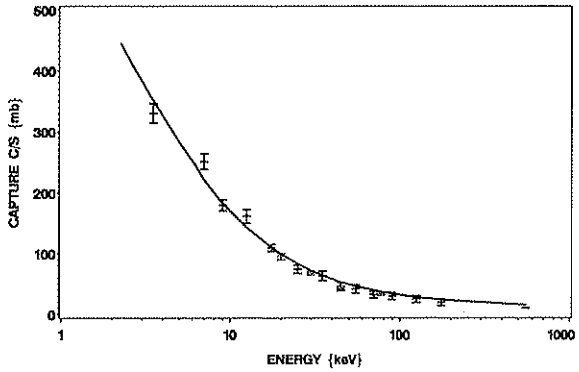

Fig. 1. Least-squares fit of ^{91}Zr capture data in the unresolved energy region [15].

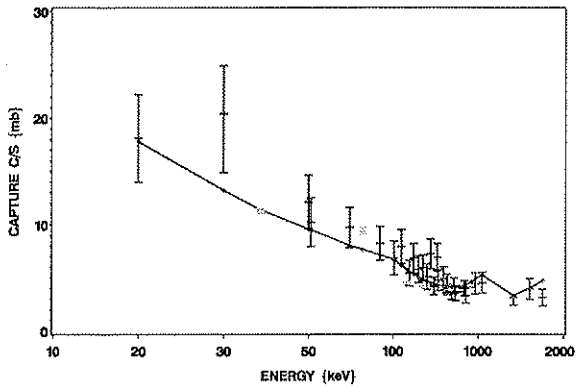

Fig. 2. Least-squares fit of ^{124}Sn capture data in the unresolved energy region [15]. The average p-wave capture width determined here for the first time is 93.3 ± 3.2 meV.

are given in [9–12]. Combined with recent information on the average neutron-resonance parameters, and supplemented by systematics displayed in [13], these measurements made it possible to obtain, for the first time, reliable values for the s- and p-wave average radiative widths, $\langle \Gamma_{\gamma 0} \rangle$ and $\langle \Gamma_{\gamma 1} \rangle$, in an extensive mass region.

Based on the Lane-Lynn formulation [14] for the average capture cross section in the unresolved resonance region, a least-squares fitting program was written to determine $\langle \Gamma_{\gamma 0} \rangle$ and $\langle \Gamma_{\gamma 1} \rangle$ for nuclei in the mass region from ^{45}Sc to ^{243}Am. This analysis included the s-, p-, and d-wave contributions to the capture cross section. An iterative procedure was followed wherein changes within the uncertainty limits of the input average resonance parameters were made until calculated initial and final cross sections converged to the measured cross section. Through this procedure, $\langle \Gamma_{\gamma 1} \rangle$ values were obtained for the first time, particularly for A>140. Examples of such fits are illustrated in Fig. 1- Fig. 3 for ^{91}Zr, ^{124}Sn, and ^{232}Th, respectively. In Fig.1, the data points for ^{91}Zr represent measurements carried out at ORNL and at the Tokyo Institute of Technology; those in Fig. 2 for ^{124}Sn represent recent data from KFK and older data [15]; those for ^{232}Th represent the recent CERN measurements [15]. The obtained capture widths for these cases are included in Table 1 along with others.

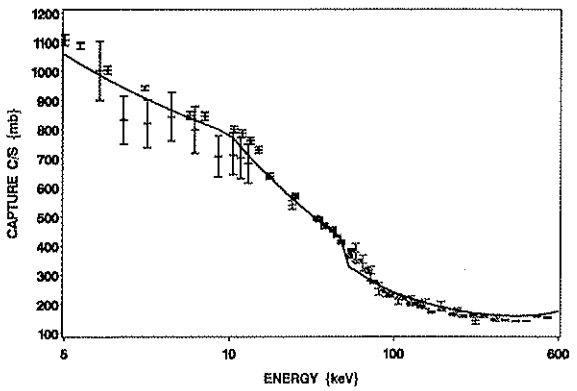

Fig. 3. Least-squares fit of ^{232}Th capture data in the unresolved energy region [15]. The average p-wave capture width determined here for the first time is 24.8 ± 0.5 meV.

3. RESULTS

Table 1 summarizes some of the derived results for $\langle \Gamma_{\gamma 0} \rangle$ and $\langle \Gamma_{\gamma 1} \rangle$ as examples; the details will be published elsewhere [16].

Our present knowledge of the neutron radiative process shows that the total average radiative width for p-wave neutrons is composed of two major components: one related to single particle (SP) effects, $\Gamma_{\gamma 1}(SP)$, the other to a statistical part, $\Gamma_{\gamma 1}(GDR)$, induced by the tail of the giant dipole resonance (GDR) [4]. Thus one can write for the individual, as well as the average, radiative widths of neutron resonances: $\langle \Gamma_{\gamma 1} \rangle = \langle \Gamma_{\gamma 1}(SP) \rangle + \langle \Gamma_{\gamma 1}(GDR) \rangle$ [17]. Since $\langle \Gamma_{\gamma 1}(SP) \rangle$ is linearly related to the neutron strength function [18], which in turn contains $S^1_{1/2}$ and $S^1_{3/2}$ structures [6,7], then it immediately follows that similar structures are expected to be observed in the average p-wave radiative widths of $\langle \Gamma_{\gamma 1}(SP) \rangle$. However, radiative widths contain dependences on excitation energy, average level spacing, nuclear-level density parameter, shell effects, pairing effects and deformations. To eliminate these effects, the p-wave radiative widths are divided by the s-wave counter part to form a dimensionless quantity, $R_{ps}(A) = \langle \Gamma_{\gamma 1} \rangle / \langle \Gamma_{\gamma 0} \rangle$. The results are displayed in Fig. 4 versus A for nuclei in the mass range from ^{40}Ca to ^{243}Am. It is important to note that in some cases where the s-wave strength function values are quite small, the average capture cross section in the keV region is not sensitive to $\langle \Gamma_{\gamma 0} \rangle$. For such cases,

the values in [13] are adopted. In addition, when average neutron capture measurements were unavailable, the s- and p-wave average capture widths, derived from the resolved resonance parameters [13], are adopted and the ratio $\langle\Gamma_{\gamma 1}\rangle\langle\Gamma_{\gamma 0}\rangle$ is presented in the figure. For comparison, the optical-model calculations representing the p-wave neutron strength function data, S_1, [13] in units of 0.4×10^{-4}, are displayed by the red line. As illustrated, four striking features emerge: (a) three resonance-like structures, located at about A = 92, 112, and 124, are clearly evident (b). Away from these structures, $R_{ps}(A)$ approaches a constant value, and (c) $R_{ps}(A)$ is highly correlated with S_1 for $80 < A < 140$, (d) there is a hint of a possible structure, peaking at about A = 230, in the vicinity of the 4p single particle state. At this point, it is significant to stress that the correlation coefficient for R_{ps} and S_1 is 0.60 for $80 < A < 140$ when all the data points are included, whereas it increases significantly to 0.74 when data points with $R_{ps} > 1.0$ are not included. The first, second, and third observations led to the representation of the data by two resonance terms [19–21] in addition to a constant background term,

$$\frac{\langle\Gamma_{\gamma 1}\rangle}{\langle\Gamma_{\gamma 0}\rangle} = B_{GDR} + \frac{K3}{(A - A_{3/2})^2 + (\frac{W_{p3/2}}{2})^2} + \frac{K1}{(A - A_{1/2})^2 + (\frac{W_{p1/2}}{2})^2} \quad (1)$$

where B_{GDR} is a background term, $\langle\Gamma_{\gamma 1}(GDR)\rangle/\langle\Gamma_{\gamma 0}\rangle$, subsequently verified on theoretical grounds to be equivalent to the statistical contribution of the tail of the giant-dipole resonance (GDR). The two resonance terms correspond to the single particle component of the p-wave radiative width. $A_{3/2}$, $A_{1/2}$ correspond, respectively, to the mass numbers where the two resonance peaks are located; K3, K1 are related to the single-particle reduced widths; $W_{p3/2}$ and $W_{p1/2}$ correspond to the damping widths, in mass units, for the first and second observed structures in Fig 4. The latter values are associated with the imaginary part of the optical-model potential [19,20], which accounts for the p-wave neutron strength function data.

At this point, it is reasonable to question whether the resonance terms are a manifestation of the effects of single-particle states of the entrance channel or doorways (2p-1h) of the exit channel. The answer can be found upon determining, in MeV units, the magnitude of the damping widths of the two observed structures and comparing them with the optical-model values.

On this basis, a least-squares fitting procedure to the experimental values, $\langle\Gamma_{\gamma 1}\rangle/\langle\Gamma_{\gamma 0}\rangle$, is carried out in terms of Eq. 1 for the mass region $A = 40 - 140$. The results yielded the following values: $B_{GDR} = 0.50 \pm 0.04$; $A_{3/2} = 92.2 \pm 1.6$, $A_{1/2} = 112.4 \pm 1.1$; K3 = 102 ± 20, K1 = 27 ± 10; $W_{p3/2} = 19.2 \pm 2.0$, $W_{p1/2} = 11.0 \pm 2.4$. Note that the mass splitting determined here, $\Delta A = 20.2 \pm 1.9$, is in very good agreement with [6,7]. At this point, it is significant to note that when the fitting is extended to A=243, then $B_{GDR} = 0.55 \pm 0.02$, which is in good agreement with the previous determination within two standard deviations.

To convert from "A" units to MeV units, the invariant quantity, R^2V_0 = constant [18] is used along with the condition that $V_0 = 43.5$ MeV and $R = 1.35A^{1/3}$ fm, which well described both the S_0 and S_1 data (refer to Fig. 2.1 - Fig 2.2 of Ref. [13]). Then, it follows that

$W_{p3/2} = 5.1 \pm 0.5$ MeV,

$W_{p1/2} = 3.0 \pm 0.7$ MeV,

$A_{1/2} - A_{3/2} = 5.7 \pm 0.4$ MeV

The quoted uncertainties reflect only those due to the fitting procedure, and do not include those due to the conversion procedure. A verification of the last result is also provided by spherical optical model calculations which gives a a value of 6.29 MeV [22], when the $p_{3/2}$ and $p_{1/2}$ single particle states are placed at A = 90 and 112 respectively. In addition, these results are in reasonable agreement

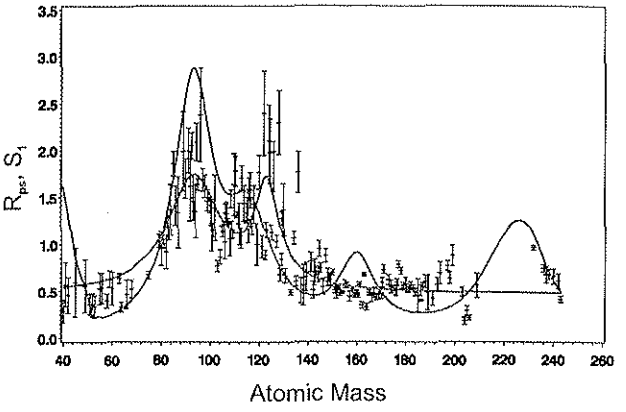

Fig. 4. The average p-wave radiative widths, normalized to the corresponding s-wave widths, are shown versus mass number for nuclei ranging from ^{40}Ca to ^{243}Am. The red line represents the least-squares fit to the data in terms of Eq. 1. The green curve, multiplied by 0.4×10^4, represents the p-wave neutron strength function data, S_1. The two strong resonance structures at A = 90 and 112 are identified as the $p_{1/2}$ and $p_{3/2}$ components of the single-particle 3p state. The resonance structures in S_1 at A = 160, 225 correspond to the 4p single-particle state split by deformation; see [2]. Note that capture data for unstable nuclei $A = 211 - 229$ are not available.

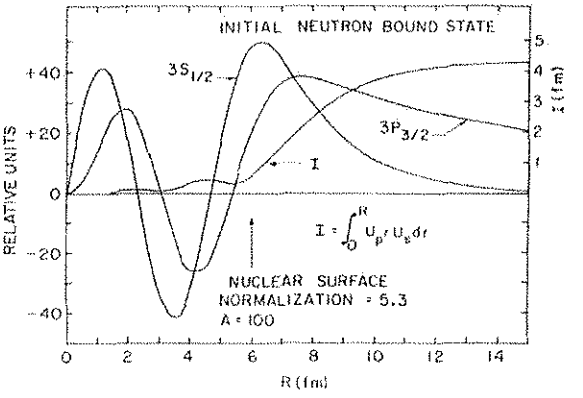

Fig. 5. Dipole Resonance Integral for an incident 3p-wave neutron captured into an s-orbit. Note that the dominant contribution to the dipole integral comes from the region external to the nucleus.

with the optical-model potential parameters describing the S_0 and S_1 data [13]: W_D(surface absorption potential) = 5.7 MeV and spin-orbit term V_{SO} = 8.0 MeV. Although different optical model geometry was used, it is of interest to compare the $p_{1/2}$ and $p_{3/2}$ damping widths derived here with those obtained by the method of transformation from multilevel R-matrix to optical model parameters for the total cross section of ^{32}S: $W_D(p_{1/2}) = 2.6 \pm 1.1$ MeV and $W_D(p_{3/2}) = 4.5 \pm 1.8$ MeV [24].

The findings that $W_{p3/2} = 5.1 \pm 0.5$, $W_{p1/2} = 3.0 \pm 0.7$ MeV, and $A_{1/2} - A_{3/2} = 5.7 \pm 0.4$ MeV = V_{SO} strongly suggest that the data of Fig. 4 are a manifestation of single-particle, but not doorway, effects. Note that theoretical expectation of the magnitude of the damping width of a doorway state in this mass region is of the order of 100 keV [18]. Furthermore, it is most noteworthy that the present results show the strong correlations between p-wave radiative widths and p-wave reduced neutron widths of resonances in the mass region $A = 80-130$, in agreement with measurements [17].

4. DISCUSSION

In the past years, correlations between capture and reduced neutron widths were attributed to valence neutron-resonance capture [18,25]. The first observation and quantitative verification for such a reaction mechanism was made at the fast chopper-facility of the HFBR at BNL [26] for the ^{92}Mo and ^{98}Mo resonances, and then at ANL for a target of ^{91}Zr by utilizing the threshold photo-neutron technique [27]. Further support for this interpretation comes from transmission and capture measurements of Ref. [28, 29] for a target nucleus, ^{88}Sr. The former group [28] reported the following significant results: $S^1_{1/2} = 2.13 \pm 0.4$, $S^1_{3/2} = 6.25 \pm 0.85$, and correlation coefficients between capture widths and reduced neutron widths, $\rho(\Gamma_{\gamma\lambda}, \Gamma^1_{n\lambda}) = 0.55 \pm 0.09$, 0.59 ± 0.9, for $p_{1/2}$, $p_{3/2}$ resonances, respectively and $\rho(\Gamma_{\gamma\lambda}, \Gamma^0_{n\lambda}) = 0.23 \pm 0.06$ for $s_{1/2}$ resonances, . The latter group's [29] corresponding correlation coefficients were: $0.40^{+0.23}_{-0.29}$, $0.83^{+0.09}_{-0.17}$, and $0.57^{+0.14}_{-0.18}$ for the $p_{1/2}$, $p_{3/2}$, and the total p components, respectively. In addition, for the target nucleus ^{89}Y, Ref. [30] found $\rho(\Gamma_\gamma, \Gamma^1_n) = 0.71 \pm 0.25$ for p-wave resonances and $\rho(\Gamma_\gamma, \Gamma^0_n) = 0.01$ for s-wave resonances. On theoretical grounds the s-wave correlation coefficient in this mass region is expected to be insignificant since the 3s single-particle state is located at A = 50.

Next, the interpretation of the background term, $B_{GDR} = 0.50 \pm 0.05$, which is surmised to be the statistical component of the neutron radiative mechanism is considered. This value can be estimated on the basis of the generalized Landau-Fermi liquid model [8]. This model was described previously in detail, and was shown to account successfully for the E1 gamma-ray strength function data for both spherical and deformed nuclei. It also was utilized to calculate the average s-wave radiative widths [8,13] of neutron resonances. The central point of this model is the inclusion of an additional term, the dipole-quadrupole interaction, for describing the damping width of the giant-dipole resonance,

$$\Gamma_g(E_\gamma, T, \beta_2) = C(E_\gamma^2 + 4\pi^2 T^2) + \Gamma_{dq}(\beta_2, E_\gamma) \qquad (2)$$

where E_γ is the gamma-ray energy, T is the thermodynamical nuclear temperature, β_2 is the dynamic quadrupole deformation parameter of the nucleus, C is a normalizing constant determined as in Ref. [31] by the condition $\Gamma_g(E_g, T = 0, \beta_2) = \Gamma^0_g$ (damping width of the GDR built on the ground state), and $\Gamma_{dq}(\beta_2, E_\gamma)$ is expressed by [8]

$$\Gamma_{dq}(\beta_2, E_\gamma) = 2.35 \sqrt{\frac{5}{8\pi}} E_\gamma \beta_2 (1 + \frac{E_2}{E_\gamma})^{1/2} \qquad (3)$$

where E2 is the energy of the first E2 excited state of the compound nucleus for spherical nuclei; for deformed nuclei, an average value of the energies of the β and γ

Table 1. The s- and p-wave radiative widths, $\langle\Gamma_{\gamma 0}\rangle$ and $\langle\Gamma_{\gamma 1}\rangle$, derived in the present work from capture cross section measurements in the unresolved resonance region. The last two columns include the experimental and theoretical values for the ratio $R_{ps}(A)$, as calculated by the generalized Fermi-liquid model, respectively.

nucleus	$\langle\Gamma_{\gamma 0}\rangle$ (meV)	$\langle\Gamma_{\gamma 1}\rangle$ (meV)	$R_{ps}(A)_{exp.}$	$R_{ps}(A)_{theo.}$
^{40}Ca	1500 ± 900	360 ±90	0.24±0.19	0.29
^{55}Mn	750 ± 150	400 ±100	0.53±0.17	0.29
^{74}Se	250 ± 20	169 ±7	0.68±0.07	0.44
^{90}Zr	124 ± 15	211 ±7	1.70±0.21	0.17
^{91}Zr	108 ± 18	252 ±16	2.33±0.16	0.19
^{122}Sn	44 ± 8	105.4±3.9	2.40±0.45	0.23
^{124}Sn	50 ± 4	93.3 ±3.2	1.87±0.16	0.24
^{151}Sm	96.0 ±1.6	49.2±9.1	0.51±0.13	0.43
^{151}Eu	93.2 ±1.0	44.6±5.1	0.48±0.06	0.52
^{153}Eu	84.7 ±1.0	43.2±4.4	0.51±0.05	0.55
^{155}Gd	102.6 ±1.2	57.1±4.0	0.56±0.04	0.44
^{157}Gd	103.5 ±1.6	53.7±6.4	0.52±0.06	0.47
^{159}Tb	103.5 ±2.3	47.3±3.9	0.46±0.04	0.52
^{161}Dy	107.6 ±1.3	61.2±2.8	0.57±0.03	0.45
^{163}Dy	103.4 ±1.4	69.8±2.9	0.68±0.03	0.49
^{167}Er	92.0 ±2.5	44.0±4.3	0.47±0.03	0.49
^{169}Tm	90.4 ±3.9	52.7±4.2	0.47±0.05	0.54
^{176}Lu	65.1 ±1.2	33.0±3.7	0.51±0.06	0.54
^{179}Hf	66.4 ±0.8	39.4±2.4	0.59±0.04	0.47
^{181}Ta	64.3 ±0.9	33.4±2.0	0.52±0.03	0.53
^{184}W	52.1 ±1.5	25.6±1.8	0.49±0.04	0.47
^{186}W	52.0 ±2.2	26.5±3.1	0.51±0.06	0.53
^{205}Tl	1190 ±160	330 ±50	0.28±0.06	0.20
^{232}Th	25.6 ±0.5	24.8±0.5	1.02±0.03	0.51
^{236}U	27.6 ±1.3	20.6±0.5	0.75±0.04	0.53
^{238}U	23.6 ±4.0	16.1±1.3	0.68±0.06	0.52
^{237}Np	41.2 ±0.9	26.4±3.5	0.68±0.09	0.49
^{240}Pu	33.0 ±1.0	21.9±2.4	0.66±0.08	0.54
^{242}Pu	28.2 ±3.2	17.1±1.2	0.61±0.08	0.54
^{243}Am	38.0 ±1.3	19.6±1.2	0.52±0.07	0.52

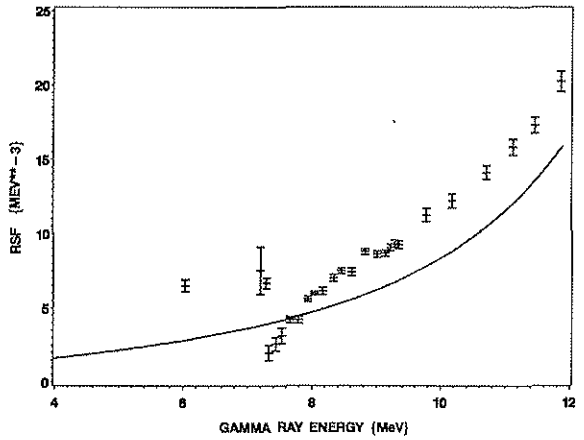

Fig. 6. ^{90}Zr gamma strength function values obtained from gamma-ray spectra measurement [27,12] and photonuclear data [34]. As shown, enhancements over the predictions of the GDR (solid line) are found in both measurements.

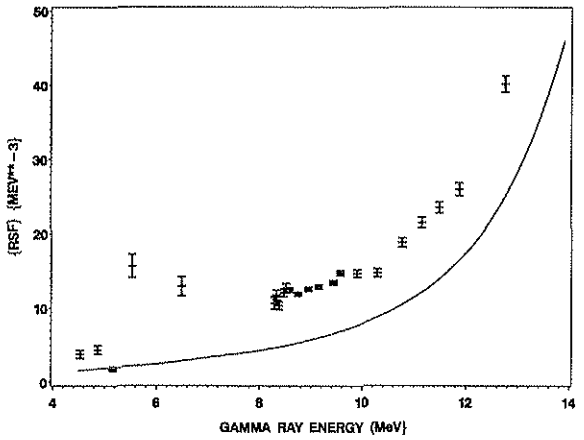

Fig. 7. ^{94}Zr gamma strength function derived from gamma-ray spectra measurement [35] and photonuclear data [34]. Enhancements over the prediction of the GDR, represented by the solid line, is observed

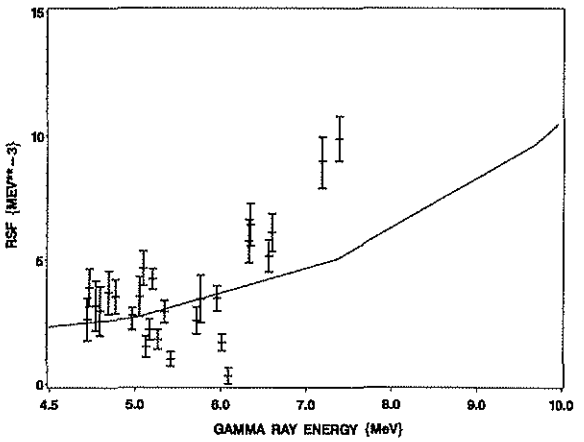

Fig. 8. ^{94}Mo gamma strength function derived from gamma-ray spectra measurement [35] [34]. Enhancement of gamma strength over the prediction of the GDR, represented by the solid line, is observed.

vibrational states is assumed. The significance of the dipole-quadrupole interaction term and the role it plays in the damping width of the GDR is demonstrated in [23].

On phenomenological grounds, this study revealed that the p-wave radiative widths can be accounted for by stipulating that p-wave neutrons excite dominantly the dipole-quadrupole surface mode, but not the giant dipole resonance mode. Some justification for this notion is derived from Fig. 5 representing the radial dependence of the dipole integral, I. As illustrated, the dominant contribution to I is coming from the region external to the nucleus. By setting $C = 0$, in Eqs. 2 and following the procedure described in [8], the calculated p-wave radiative widths are estimated. For s-wave neutrons, on the other hand, the two terms on the right-hand side of Eq. 2 contribute to the radiative neutron reaction. As a result, on the basis of this model, $\langle\Gamma_{\gamma 1}\rangle/\langle\Gamma_{\gamma 0}\rangle$ can be readily calculated. The last column of Table 1 includes the calculated ratio R_{ps}(A). As shown, the theoretical values range from 0.17 for ^{90}Zr to 0.55 for ^{153}Eu and nicely follow the trend of the experimental values. In addition, in the actinide region, the high experimental values for R_{ps}(A) ranging from 1.04 for ^{232}Th to 0.52 for ^{243}Am can be attributed to the effect of the 4p single-particle state, which was predicted by the optical-model at A=225 [3,13].

Additional support for single particle effects in the capture process comes from gamma-ray spectra measurements and threshold and above-threshold photonuclear measurements [27,34]. The gamma strength functions for ^{90}Zr, ^{94}Zr,^{94}Mo and ^{98}Mo are derived from such measurements and dispayed in Fig. 6 - Fig. 9. As is evident, there is an enhancements over the prediction of the extrapolation of the GDR.

By contrast, as pointed out previously, the enhacements of the p-wave radiative widths in the Sn-Ba region are not due to single particle effects since these quantities are not correlated with S_1. Additional support for this comes from gamma-ray spectra measurements in the Sn-region where it was shown that the measured partial radiative widths cannot be accounted for in terms of the valence model [36]. The source for these enhancements is probably due to the Pygmy dipole Resonance observed in nuclear resonance florescence measurements.

5. CONCLUSIONS

In summary, the data presented here have expanded our knowledge and understanding of the average p-wave capture widths of neutron resonances. This was achieved by deriving, for the first time, $\langle\Gamma_{\gamma 1}\rangle$ values from high-precision neutron capture measurements in the unresolved

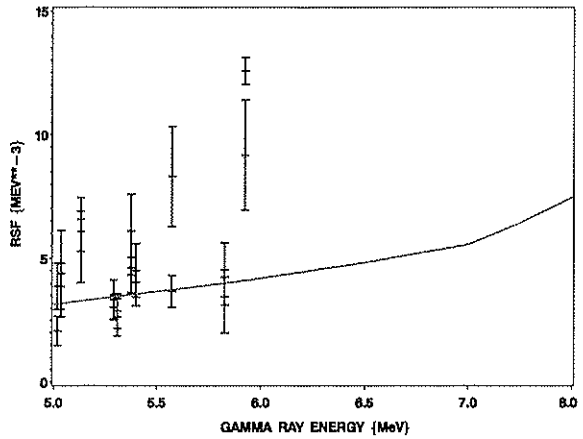

Fig. 9. ^{98}Mo gamma strength function derived in the present study from gamma-ray spectra measurement [35] [34]. Enhancement of gamma strength over the prediction of the GDR, represented by the solid line, is also observed here.

energy region and interpreting them in terms of the single-particle model, as well as the giant-dipole model. The two resonance-like structures observed here for the first time at mass numbers 92 and 112 are interpreted in terms of the splitting of the 3p single-particle state into the $p_{1/2}$ and $p_{3/2}$ components; the strength of the spin-orbit potential of the optical-model was assessed as 5.7 ± 0.4 MeV, in excellent agreement with other determinations [32,33]: 6.2 ± 1.0 MeV and 6.0 MeV. The origin of the observed structure about A=124, which is found uncorrelated with S_1, is probably due to the Pygmy Giant Resonance. The background term B_{GDR} is accounted for in terms of the generalized Fermi liquid model demonstrating that p-wave resonances are partially decoupled from the giant dipole resonance. The present results demonstrate and give a new dimension to the generalized Fermi liquid model [8].

ACKNOWLEDGMENTS

The author is greatly indebted to G. E. Brown and A. M. Lane for their encouragements throughout the years, to P. Oblozinsky and M. Herman for their support and D. J. Millener for stimulating discussions; the assistance of B. Pritychenko and M.T. Pigni with Latex are appreciated. Work at Brookhaven National Laboratory was sponsored by the office of the U.S. Department of Energy under contract No. DE-AC02-98CH10886 with Brookhaven Science Associates, LLC.

REFERENCES

[1] H. Feshbach, C. E. Porter, and V. F. Weiskopf, Phys. Rev. 96, 448 (1954).
[2] B. Buck and F. Perey, Phys. Rev. Lett. 8, 444 (1962).
[3] S. F. Mughabghab, Neutron Cross Sections and Technology, J. A. Harvey and R. L. Macklin, editors, p. 386 Knoxville, Tennessee, 1971.
[4] S. F. Mughabghab, Statistical Properties of Nuclei (editor J.B. Garg) Plenum Press 1972 p. 291.
[5] S. F. Mughabghab, Neutron Cross Sections: Resonance Parameters and Thermal Cross Sections, Vol 1 part B Z=61-100, Academic Press Orlando 1984.
[6] A. B. Popov and G. S. Samosvat, Yad. Fiz., 45, 1522 (1987).
[7] Zo In Ok, V. G. Nikolenko, A. B. Popov, and G. S. Samosvat, JETP Lett., 38, 363 (1983).
[8] S. F. Mughabghab and C. L. Dunford, Phys. Letters B 487, 155 (2000).
[9] R. L. Macklin, Astro. and Space Science, 115, 71, (1985).
[10] U. Abbondanno, G. Aerts, Alvarez-Velarde et al., Phys. Rev. Lett. 93, 161103 (2004).
[11] K. Wisshak, F. Voss, F. Kaeppeler, K. Guber et al., Phys. Rev. C, 52, 2762 (1995).
[12] K. Ohgama, M. Igashira, and T. Ohsaki, J. Nuc. Sci. Tech.,42, 333 (2005).
[13] S. F. Mughabghab, Atlas of Neutron Resonances: Resonance Parameters and Thermal Cross Sections Z=1-100, Elsevier, Amsterdam 2006.
[14] A. M. Lane and J. E. Lynn, Proc. Phys. Soc. (London) A70, 557 (1957).
[15] Experimental Nuclear Reaction Database (EXFOR), http://www.nndc.bnl.gov/exfor.
[16] S. F. Mughabghab, in preparation.
[17] S. F. Mughabghab, Lectures at the Third International School on Neutron Physics, Alushta, Crimea, USSR, JINR(Dubna) Report No Dz-11787 p.328 (1978).
[18] J. E. Lynn, The Theory of Neutron Resonance Reactions, Clarendon Press, Oxford 1968, and references therein.
[19] A. M. Lane, R. G. Thomas, and E. Wigner, Phys. Rev. 98, 693 (1955).
[20] A. M. Lane, Phys. Lett. B 33, 274, (1970).
[21] G. E. Brown, Rev. Mod. Phys., 31, 893 (1959).
[22] D. J. Millener, private communication (2008).
[23] S. F. Mughabghab, Capture Gamma-Ray Spectroscopy and Related Topics, Editors: J. Kvasil, C. Cejnar, and M. Kriticka, p. 252, World Scientific 2003.
[24] C. H. Johnson and R. R. Winters, Phys. Rev. C 21, 2190 (1980).
[25] A. M. Lane and S. F. Mughabghab, Phys. Rev. C 10, 412 (1974).
[26] S. F. Mughabghab, R. E. Chrien, O. A. Wasson, G. W. Cole, and M. R. Bhat, Phys. Rev. Lett. 26, 1118 (1971).
[27] R. E. Toohey and H. E. Jackson, Phys. Rev. C 9, 346 (1974).
[28] P. E. Koehler, R. R. Winters, K. H. Guber et al., Phys. Rev. C 62, 055803 (2000).
[29] B. J. Allen, R. Shelly, T. van der Veen, A. Brusegan, and G. Vanpraet, in Neutron-Capture Gamma-Ray Spectroscopy and Related Topics, p. 404, Grenoble, 1981.
[30] J. W. Boldeman, B. J. Allen, A. R. de L. Musgrove, and R. L. Macklin, Nucl. Sci. Eng. 64, 744 (1977).
[31] S. G. Kadmenskii, P. Markushev, and V. I. Furman, Yad. Fiz. 37, 277 (1982).
[32] F. D. Becchetti and G. W. Greenless, Phys. Rev. 182, 1190 (1969).
[33] D. C. Kocher and W. Haeberli, Nucl. Phys. A 196, 225 (1972).
[34] H. Utsunomiya, S. Goriely, T. Kondo et al., Phys. Rev. Lett. 100,162502 (2008).
[35] M.J. Kenny, M.L.Stelts, and R.E. Chrien, Neutron Capture Gamma-Ray Spectroscopy, Edited by R.E. Chrien and W.R. Kane, Plenum Press 646 (1979).
[36] M. R. Bhat et al. Phys. Rev. C 12, 1457 (1975).